submitted to PSI Users Meeting BV29, 5/7/99

Search for the decay $\mu^+ \to e^+\gamma$

Update and supplement to the Letter of Intent R-98-05.0

MUEGAMMA Collaboration

A. Baldini[3], C. Bemporad[3], G. Bressi[2], P. Cattaneo[2], G. Cecchet[2], F. Cei[3], F. Foroughi[4], M. Grassi[3], E. Hermes[8], S. Korenchenko[1], T. Kozlowski[6], G. Liguori[2], D. Mzavia[7], M. Moszynski[6], D. Nicolò[3], R. Pazzi[3], D. Renker[4], A. van der Schaaf[8], H. C. Walter[4], H. P. Wirtz[4], and D. Zanello[5].

1. JINR, Dubna, Russia
2. INFN, Pavia, Italy
3. University of Pisa and INFN, Pisa, Italy
4. PSI, CH-5232 Villigen PSI, Switzerland
5. INFN, Roma1, IT-00185 Roma, Italy
6. IPJ, PL 05-400 Otwock-Swierk, Poland
7. HEPI, Tbilisi State University, GE-380086 Tbilisi, Georgia
8. Physics Institute, University of Zurich, Switzerland

May 24th 1999

Abstract:

We present the progress made since PSI LOI R-98-05 towards a $\mu \to e\gamma$ set-up based on an intermediate focusing positron spectrometer and a NaI(Tl) photon calorimeter with LYSO pre-shower detector:

- The coil configuration was optimized to include the requirements of beam transport, positron suppression in the beam and positron sweeping away from the photon detectors.
- The πE5 surface muon beam was studied and neutron and gamma backgrounds were measured.
- A prototype LYSO pre-shower detector was studied *in the energy region of interest* with protons, electrons and photons.

The results give us confidence in reaching the sensitivity and background levels quoted in LOI R-98-05.

1 Introduction

This document is an update of the LOI submitted on April 1998 [1]. Since that date, studies went on and a series of experimental tests were made at PSI. A new plenary meeting of the collaboration took place on April 24th 1999; during that meeting we had to take note that it was impossible to reach an agreement between the european and the japanese groups on a common apparatus for performing the experiment; the differences concern both the electromagnetic calorimeter and the magnet, since these two items must be well integrated and compatible. Several attempts were made to find an acceptable compromise for both parties, without success. We deeply regret not to have found a way, mutually accepted, to carry on the collaboration with the japanese institutions.

The physicists signing this document want to confirm their strong interest in the measurement of the $\mu^+ \to e^+ + \gamma$ branching ratio and their intention to initiate such an experiment in the shortest possible time. To this purpose, several experimental tests were made at PSI for optimizing and defining the properties of the $\pi E5$ beam, for measuring the neutron and photon backgrounds in the experimental area, for a preliminary measurement of the energy resolution of a LYSO+NaI γ-detector. In addition to that, the present collaboration intends to proceed along these lines:

- to perform the experiment with a set-up based on a crystal calorimeter coupled with an intermediate focusing spectrometer;
- submit a full proposal by the end of 1999;
- complete and define the collaboration at the same date;
- complete, before the end of the year, the background measurements preliminary to the experiment and complete the full study of the electromagnetic calorimeter prototype.

The motivations for a new measurement of the $\mu^+ \to e^+ + \gamma$ branching ratio B, at a level of $B \approx 10^{-14}$, were given in the LOI and maintain all their interest; a few theoretical papers [2, 3, 4], which came out during last months, confirmed that picture. The final and improved limits on B ($B < 1.2 \times 10^{-11}$; $90\,\%$ $C.L.$) were recently published by the MEGA collaboration [5].
This document contains some information on the proposed set-up for the experiment; we present results on the beam measurements and on the neutron and gamma background measurements.

2 The proposed set-up

2.1 Beam transport. Positron sweeping

The principle of operation of the proposed intermediate focusing spectrometer is described in our Letter of Intent. Here we will discuss:

- the transport of the muon beam to the experimental target and
- the sweeping of decay positrons away from the photon calorimeter.

For this purpose the coil geometry upstream of the target has been modified. By raising the field in the coil already existing in this region and by introducing an additional small coil with opposite field just before the target (see fig.4) it was possible to reduce the field along the beam axis, important to maintain the quality of the beam focus at the target, and at the same time raise the magnetic field integral between target and photon calorimeter, important to keep positrons away from the calorimeter. It was possible to do this in such a way that the field distribution seen by positrons accepted by the spectrometer remains unchanged. Fig.1 shows the field distribution along the symmetry axis.

Assuming the use of a surface, rather than a sub-surface beam, the muons would have to pass trough $\approx 1\ mm$ of CH_2 moderator before reaching the $100\ mg/cm^2$ target. Only muons with momenta below $15\ MeV/c$ would stop in such target. By positioning half of the moderator material in the last bending magnet the positron contamination can be reduced from typically $1:1$ to $1:100$ (see below). The remainder of the moderator would be placed as close to the target as possible to minimize the distortion of the beam focus.

Fig.2 shows the trajectories of $60\ MeV/c$ positrons, emitted from the target into the backward hemisphere. None escapes the region of the coils.

2.2 The electromagnetic calorimeter

The photon detector is made of two different types of inorganic scintillators constituting a pre-shower part and a shower containment part. The crystal we envisage for the shower containment is the widely used thallium doped NaI(Tl), while that for the pre-shower is a mixture (70/30) of Lutetium and Yttrium orthosilicates, doped with Cerium, LYSO(Ce) [6]; the detector is therefore a combination of a rather advanced item with another item of standard and conservative technology.

The pre-shower is required to provide the photon conversion position with a precision of few millimeters and the interaction time with a resolution of less than 200 ps.

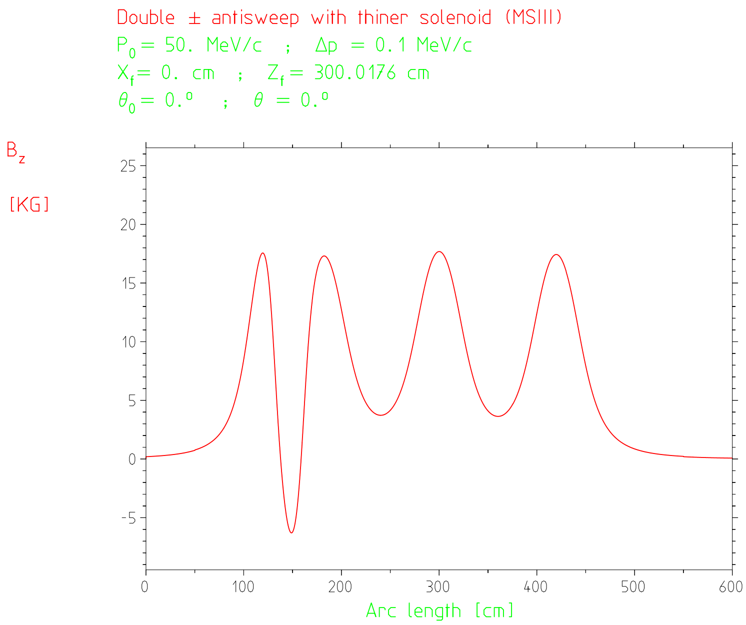

Figure 1: Field distribution along the symmetry axis.

The energy measurement combines the pre-shower and shower-containment information. The required energy resolution is at least $5\,\%$ FWHM at $52.8\ MeV$.

The performances required for the pre-shower force the choice towards recently developed luminous and fast crystals like LYSO. Its light output is $\approx\ 65\,\%$ of the NaI(Tl) and its decay time has been measured to be $48 \pm 1\ ns$.

This crystal is grown with the Tchokralsky method. Polished cylinders have at present $\sim 8\ cm$ diameter and $\sim 20\ cm$ length. The dimensions of the largest LYSO crystal we used are $10 \times 5 \times 2\ cm^3$. The pre-shower detector is designed with typical dimensions of $10\ cm$.

A cut-away view of the calorimeter is shown in fig.3 in which the thin pre-shower crown made of LYSO tiles and the large NaI(Tl) containment part are visible together with the first three super-conducting solenoids of the positron spectrometer. A lateral view of the calorimeter and of the solenoids is shown in

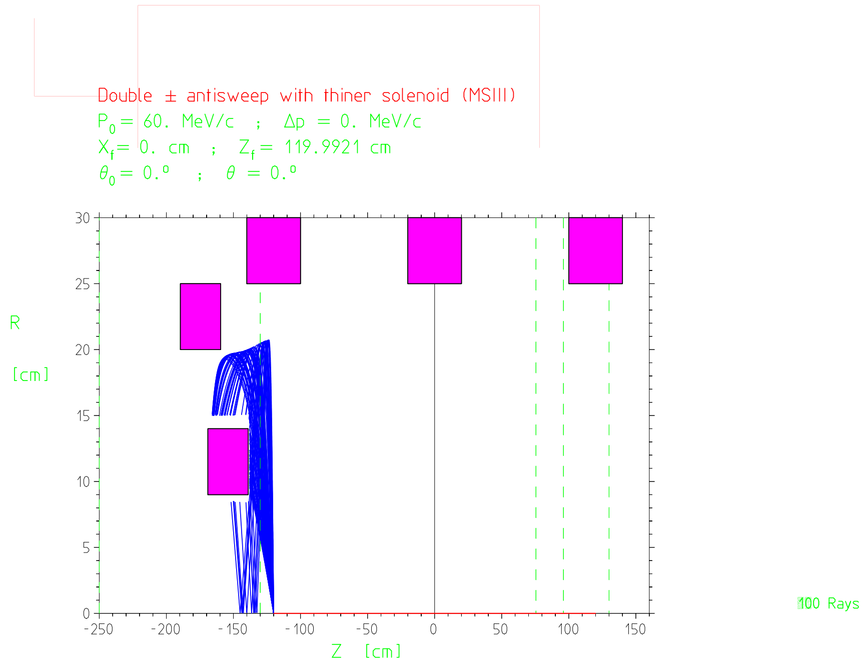

Figure 2: Trajectories of 60 MeV positrons from the target. None reaches the photon detectors.

fig.4.

The calorimeter consists of 40 identical modules of 9° azimuthal aperture whose faces are perpendicular to the line joining their center to the target where muons come to rest. The modules faces have a trapezoidal shape. The front face is composed of two LYSO tiles 11.3 cm long and 9.6 7.8 6.0 cm bases. The thickness of these tiles is 3 cm (corresponding to 1 mass attenuation length at 52.8 MeV). The depth of the following NaI crystal (again subdivided into two pieces) is 31 cm corresponding to 12 radiation lengths. The distance from the pre-shower to the target is 72 cm and the solid angle fraction covered by the calorimeter is 8.7%.

The volumes of the pre-shower and of the NaI calorimeter are 21,600 and 446,000 cm^3; their weights are 140 and 1430 Kg respectively.

We envisage a frontal read-out of the pre-shower by means of 12 Hamamatsu R5900-U PMT's per module, while each NaI module will be read from the back by two 4″ PMT's.

We are studying a different design which would eliminate the need of PMT's in front of the calorimeter. In this scheme the LYSO would be subdivided in long thin

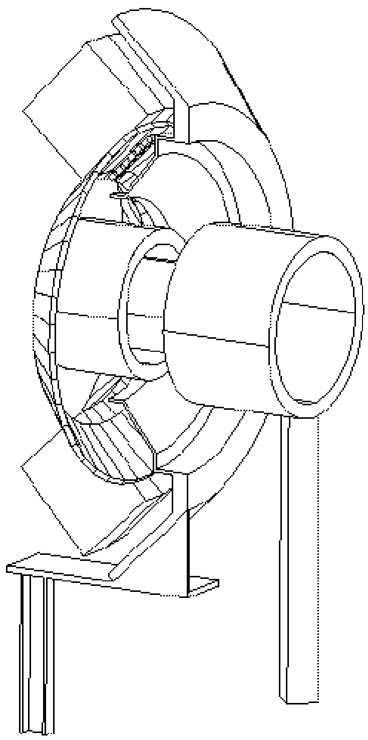

Figure 3: Cut-away layout of the calorimeter.

bars ($\sim 3 \times 3 \times 20\ cm^3$) read by one PMT at both sides. The position resolution which can be reached in this way depends on the non-uniformity of the LYSO crystals; we plan to measure it experimentally.

3 Results of beam tests

The experiment will make use of a beam of μ^+ originating in the decay of π^+ stopping close to the surface of the production target. Muons from pion decay at rest have a momentum of 29.79 MeV/c. The interactions of these muons inside the graphite production target result in a continuous momentum distribution. Since the range distribution of muons leaving the target is roughly constant, the momentum distribution rises steeply towards the endpoint due to the non-linear

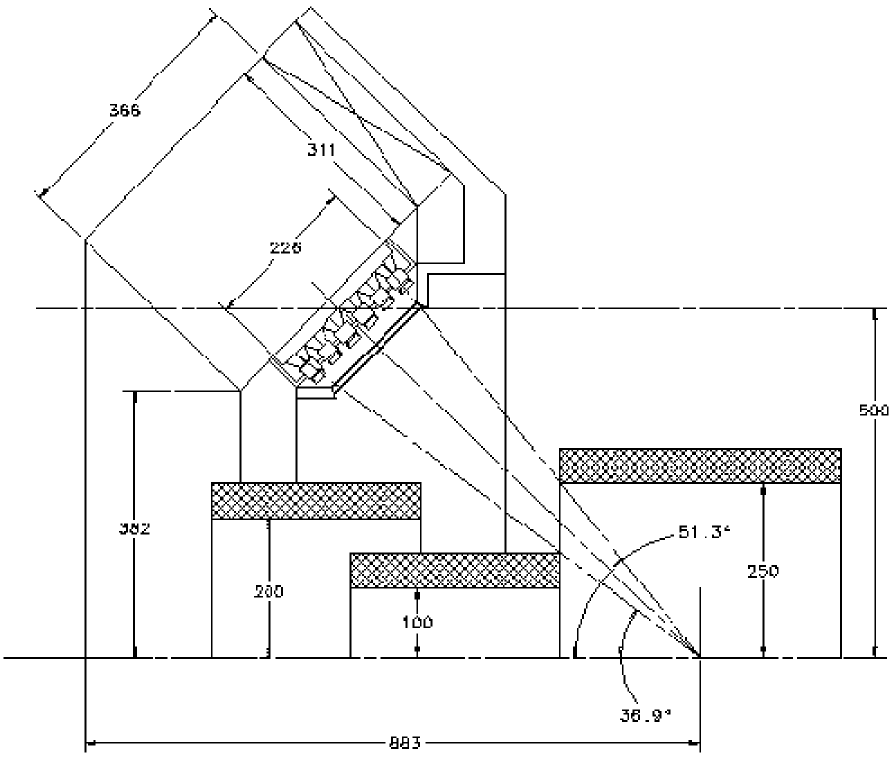

Figure 4: Lateral view of the calorimeter.

range-momentum relation, $R \propto p^{3.53}$ with p in MeV/c.

We have studied the πE5 surface muon beam using the PMC solenoid as extraction element. Fig.5 shows the general layout. The beam has a focus inside the ASC bending magnet, where a 0.5 mm CH_2 degrader could be moved into the beam. A second focus is found about 1 m after the PMC entrance where a collimator is located. Practically all muons passing the collimator reach the PMC exit where they stop. The stop rate was monitored by observing positrons from the decay $\mu^+ \rightarrow e^+\nu\overline{\nu}$ with a large NaI(Tl) detector (see Fig.6). Beam positrons were monitored with the help of a small plastic scintillator, mounted on an $x-y$ scanner, positioned behind the PMC.

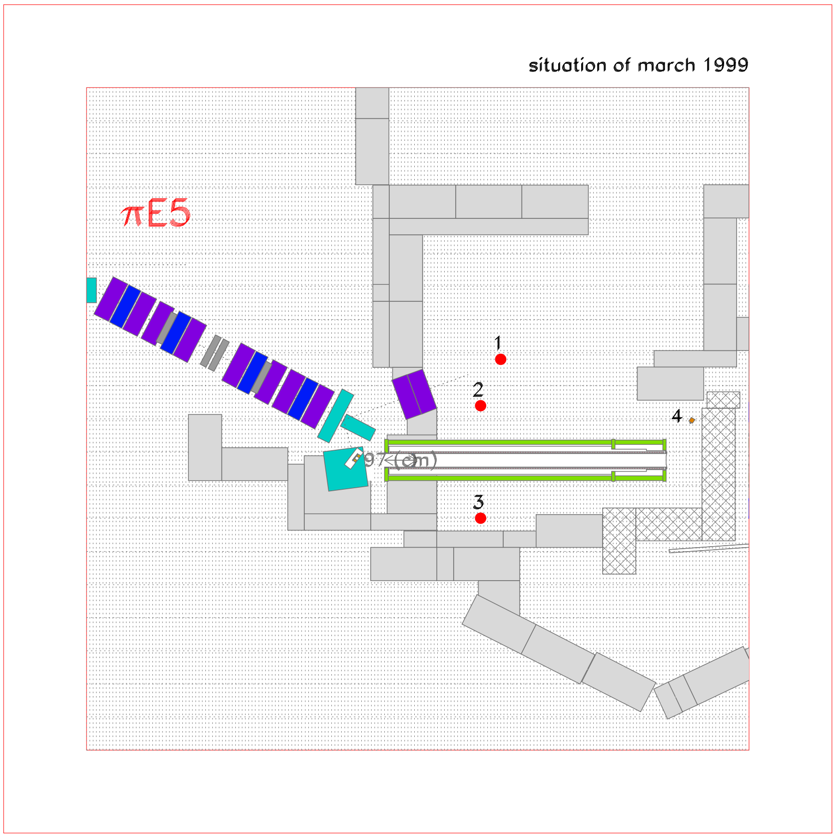

Figure 5: Setup used to study the surface muon beam.

3.1 The μ^+ and the e^+ intensities

In a first step the magnet settings were optimized for a central momentum of 28 MeV/c with the degrader moved out of the beam. The maximum muon rate that was obtained is:

$$N_\mu = 3 \times 10^8 \ s^{-1}\,, \tag{1}$$

at a proton current of 1.5 mA. One should keep in mind that the stop rate would be reduced by typically a factor 3 for a target thickness of 100 mg. The rate of positrons was determined by a scan of the beam profile and we found:

$$N_e = 5 \times 10^8 \ s^{-1}\,, \tag{2}$$

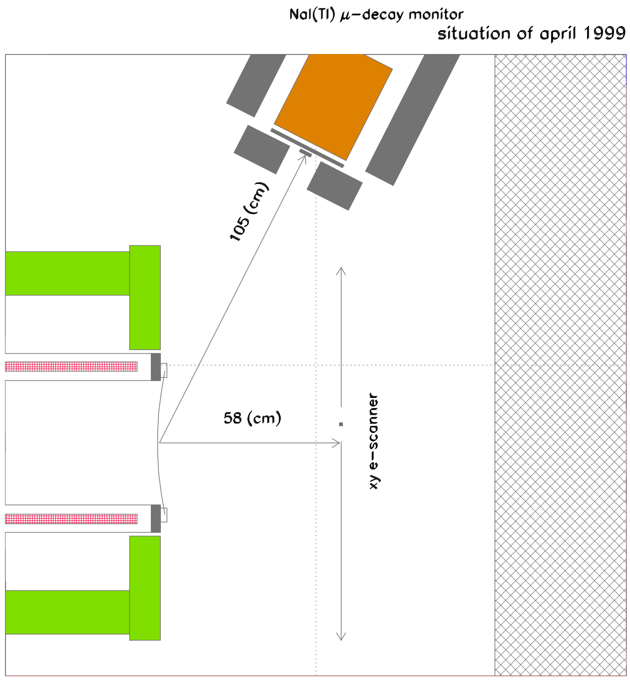

Figure 6: Detector configuration at the PMC exit.

3.2 Reducing the positron contamination

In a second step the degrader foil was moved into the beam. Whereas the positrons remain practically unaffected, the central muon momentum shifts down to 24 MeV/c. By reducing the fields in the last bending magnet (ASC) and by tuning the PMC for highest muon intensity, the positron contamination is reduced by two orders of magnitude. Fig.7 shows the rates of muons and electrons reaching the end of the PMC magnet as a function of the currents in the ASC and PMC magnets. The price for the reduction of the positron contamination is a loss of muon rate by almost a factor two:

$$N_\mu = 1.7 \times 10^8 \ s^{-1} \,. \tag{3}$$

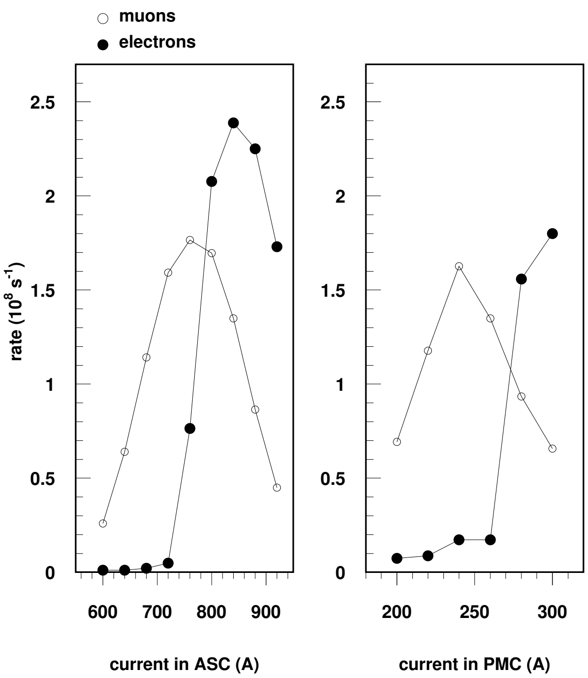

Figure 7: Yields of muons and positrons as a function of the currents in the last two beam elements. The particle discrimination is based on the separation in momentum introduced by a 0.5 mm CH_2 moderator.

The stop probability in a 100 mg target, however, would be increased in this case. Unfortunately we did not measure this quantity.

3.3 Measurement of the Michel spectrum and its Montecarlo simulation

The Michel spectrum was obtained by stopping the surface μ^+ beam in a "target" $200\,\mu$ thick and detecting the e^+ with a large NaI crystal ($11'' \times 13''$) put at a distance of $\approx$ 105 cm from the target; the set-up is shown in fig. 6; it includes collimators and scintillation counters for selecting e^+'s or for rejecting them and measuring the internal bremsstrahlung photon of the $\mu^+ \to e^+\nu_e\overline{\nu}_\mu\gamma$ decay. Several difficulties are associated with these measurements; the high beam intensity produces some pile-up, the NaI we used (7 PMT's) has AC-couplings and this produces some rate dependent spectral distortions (NaI single rates varied in the interval $30 \leftrightarrow 130\ kHz$), some magnet fringing field is present in the target region, etc.; the large size of the NaI crystal is important for fully containing the e.m. energy, but, at the same time, the large size means that the crystal is subject to a rather high and unshielded neutron background. We present in fig. 8 and fig. 9 (a blow-up of the low-energy region of fig. 8) a series of raw spectra (NaI entrance lead collimator $3.5 \times 3.5\ cm^2$) taken under various conditions: A) NaI spectrum (self-triggered), B) NaI spectrum with charged particles rejected, C) same as B), but with collimator closed by a 10 cm thick lead shield, D) same as C) but beam-shutter closed. The spectrum A) is essentially the Michel spectrum (with the

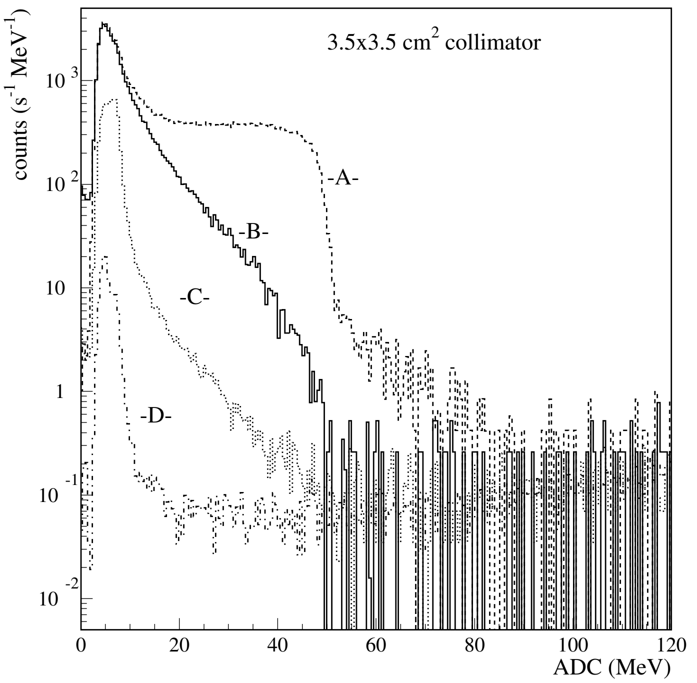

Figure 8: NaI spectra taken in various experimental configurations (see text).

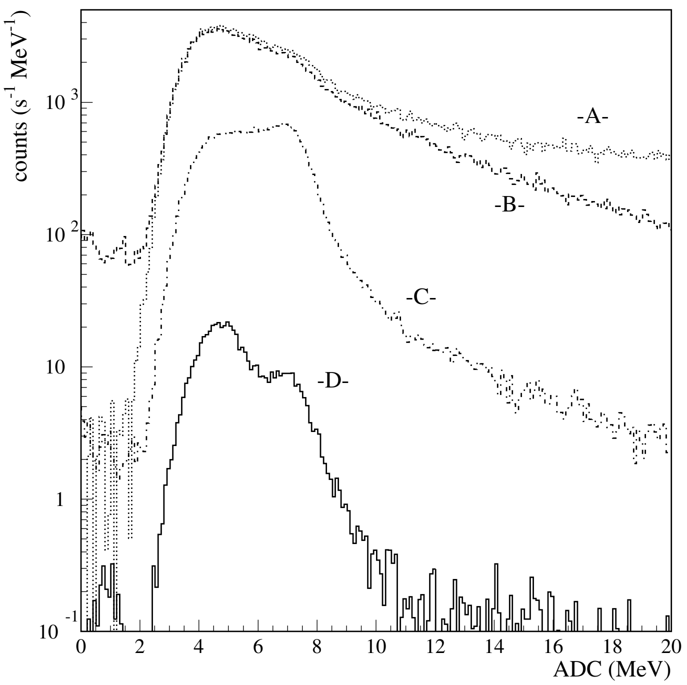

Figure 9: Low energy, larger scale detail of previous figure.

distorsions already mentioned, well reproduced by the Montecarlo simulation); at low energies the photons by internal (and some external) bremsstrahlung are contributing; contributions due to neutrons, detected by the entire crystal body, are also present and the n-capture from ^{128}I is visible as a sum of several γ-line ($6 \leftrightarrow 7\ MeV$ region). The B) spectrum is essentially the internal bremsstrahlung spectrum, whose end-point is at the maximum e^+ energy; at low energies neutron contributions are present. When γ's and e^+'s are killed (detail of spectrum C)), the neutron capture γ sum-line is more clearly visible. Neutron contributions are still visible in spectrum D); note that, at high energies, the spectra C) and D) (shutter closed) coincide; this means that cosmic rays are dominating.

A clean Michel spectrum was obtained by selecting the e^+ with a trigger given by the coincidence of a small scintillation counter and the NaI; the NaI ADC gate was 600 ns; the Michel spectrum is shown in fig. 10; there is a small tail at high energies due to pile-up; this was almost completely cancelled by comparing the charge measured with two, different duration, gates. In fig. 11 we show the Monte

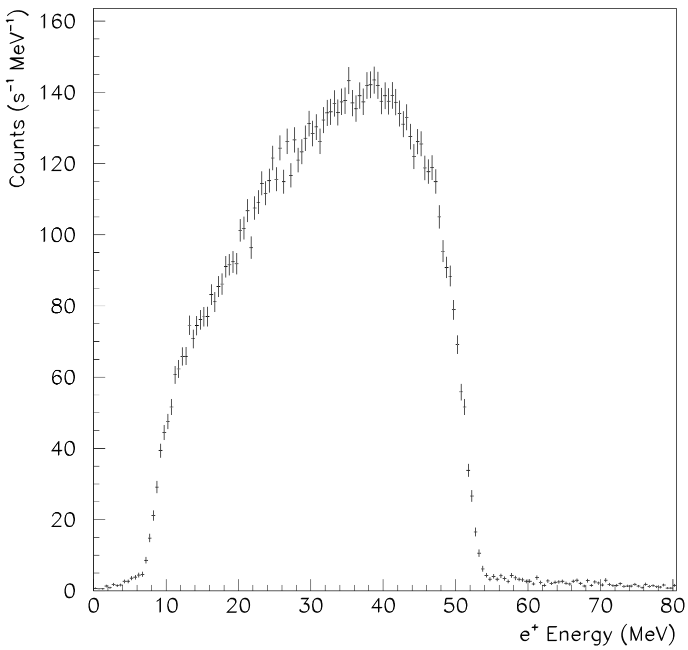

Figure 10: Experimental Michel spectrum.

Carlo simulation of the same spectrum, with the rate-dependent deformation due to the NaI capacitive coupling, and the pile-up effects visible at high energy.

It is important to note that the intensity of the surface μ^+ beam stopping in the target can only be obtained from the measurement of the Michel spectrum and of the e^+ rate in the NaI crystal; the average stopping μ^+ intensity (PSI at 1.5 mA) so obtained during this set of measurements was:

$$N_{\mu^+} = (1.4 \pm 0.2) \times 10^8 \ s^{-1}$$

We checked that this result did not depend on the NaI collimator size.

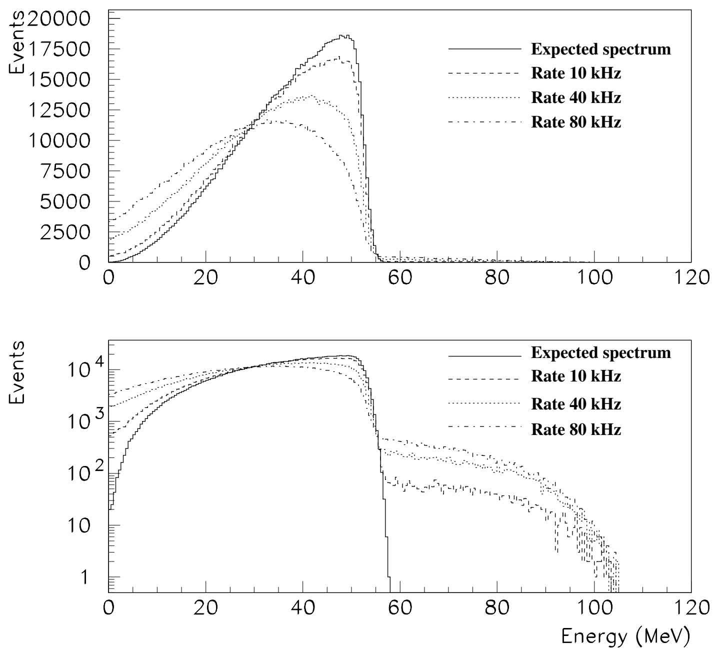

Figure 11: Simulated Michel spectrum at various acquisition rates.

4 Background measurements

We made measurements of photon and neutron fluxes at several positions in the experimental area and at variable beam intensities. In addition to the background directly generated by the μ^+ beam in the target region, these diffuse fluxes of neutrons and γ's will also be present, although partially shielded by the experimental equipment itself. Neutrons are particularly dangerous since they can produce, after moderation and capture, rather high energy γ-rays or can activate the materials present in the experiment.

4.1 Neutron background

The neutron flux (both thermal and energetic) was measured by using various devices: a $4'' \times 4''$ NaI(Tl) crystal, several NE110 plastic scintillator blocks, some activation targets, cadmium foils, etc. We used a low-threshold trigger system and a VME-based acquisition system based on a Motorola 68030 processor. Only part of the data were analysed. We start presenting the data collected with the NaI crystal. Neutrons can be captured both by ^{127}I and ^{23}Na; we rely mostly on ^{127}I since this element has peculiarities which can be put to use [7] [8] [9] [10] [11] [12] [13]:

- the neutron capture reaction $^{127}I(n,\gamma)^{128}I$ is important up to energies $T_n \approx 15\ MeV$;
- only $\approx 1 \times 10^{-3}$ of the excited ^{128}I de-excites releasing its energy as a direct transition to the ground level (maximum energy $E_c = 6.826\ MeV$);
- most of the de-excitations populate ^{128}I low-lying levels which then decay by β and $\beta + \gamma$ transitions with characteristic half life $T_{1/2} \approx 25.4\ min$;
- the energy released by these delayed transitions reaches a maximum of $E_d = 2.1\ MeV$.

Details about the ^{128}I transitions are presented in table 1. The relevant cross

Table 1: ^{128}I transitions after neutron capture. "Energy" means the energy of the γ-line and the end point of the β spectrum.

Transition	**Transition type**	**Energy (MeV)**	**Intensity (%)**
$^{128}I \rightarrow {}^{128}Xe$	β^-	2.120	76.3
$^{128}I \rightarrow {}^{128}Xe$	$\beta^- + \gamma$	$1.665(e^-) + 0.443(\gamma)$	15.5
$^{128}I \rightarrow {}^{128}Xe$	$\beta^- + \gamma$	$1.125(e^-) + 0.969(\gamma)$	2.0
$^{128}I \rightarrow {}^{128}Te$	$EC + \gamma$	0.743	6.4

sections for NaI (and CsI) activation are given in table 2. We measured the neutron fluxes by activating the NaI crystal at several positions in the experimental area and in different conditions (naked NaI, cadmium shielded NaI, paraffin hut surrounding the crystal, etc.). The locations where the activations took place are shown in fig. 5. Each exposure to the neutron flux lasted about 1 h, a time interval sufficient to approach ^{128}I "secular equilibrium". After exposure, the NaI

Table 2: Neutron cross sections (barns) at thermal energies.

Element	**σ for capture**	**Elastic scattering σ**
^{23}Na	0.528	3.319
^{127}I	6.40	4.70
^{133}Cs	28.0	7.0

crystal was put in a lead well, the device was turned-on and the crystal activity was monitored for several hours at intervals of a few minutes by using the NaI device as an "electromagnetic calorimeter". One of the activity measurements is presented in fig.12; the decreasing activity energy spectra measured by the NaI are shown at 5 minutes intervals; a ^{60}Co energy calibration spectrum is also shown (1.17, 1.33 MeV and the 2.5 MeV "sum"-line); the lowest spectrum was measured $\approx 8\ h$ after exposure, the activation decayed already and one observes again the natural (and lead shielded) radioactivity of the experimental area with its typical lines corresponding to ^{214}Bi, ^{40}K, ^{208}Tl. We present in fig. 13 the ^{128}I decay curves corresponding to various activation conditions. It is interesting to note that the repeated activation studies we made improved the ^{128}I $T_{1/2}$ value available in the literature [11]. From the data one derives a precise measurement of the thermal neutron flux and a rough determination of the non-thermal neutron flux. The link from the measured saturated activation to the neutron flux is given by an extensive Monte Carlo computation of the n-capture efficiency for thermal (ϵ_n^{th}) and non-thermal ($\epsilon_n^{nth}(T_n)$) neutrons (capture probabilities when a neutron crosses the NaI boundary and undergoes elastic scatterings and interactions); also computed by the Monte Carlo method is the NaI average efficiency for the detection of the e.m. energy released in the crystal (ϵ_{em}). The comparison of the measurements made with the naked NaI with the ones with the cadmium shielded NaI allows the separation of the contributions to the activation from thermal and non-thermal neutrons. The NaI we used has a volume $V = 824\ cm^3$ and a mass $M = 3.02\ Kg$; the saturation activity due to thermal neutrons is $A_{th} \approx 0.97\ KHz$, the one due to non-thermal neutrons is $A_{nth} \approx 1.4\ KHz$. It is worth noting that this directly measured activities are the ones that a NaI-based electromagnetic calorimeter, similar therefore to the one we intend to use for the experiment, would also have; we checked, by an ad-hoc Monte Carlo simulation, that the calorimeter energy resolution would not be appreciably affected by the neutron activation. From the measurements and from the computed efficiencies we derive a thermal neutron flux

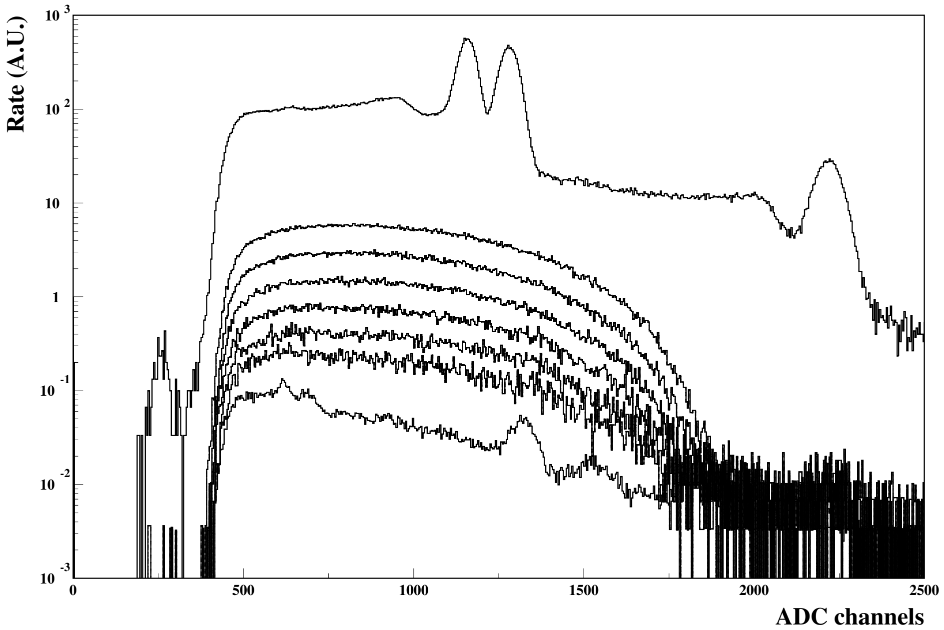

Figure 12: Example of NaI activity measurement.

of:

$$\Phi_{th} = 15 \pm 4\, n\ cm^{-2} s^{-1}$$

under the reasonable hypothesis of isotropic thermal neutron distribution. More complicate is the derivation of the non-thermal neutron flux from the data. This is so since the non-thermal neutron activation depends on the convolution of an unkwown energy dependent flux $\Phi_{nth}(T_n)$ with a known $(n\gamma)$ cross section $\sigma_{n\gamma}(T_n)$ and a computed activation and detection efficiency $\epsilon(T_n)$; some uncertainties are also related to contribution of (n,n') and (n,2n) reactions. The activation efficiency for our NaI crystal, as a function of the neutron energy, is presented in fig. 14. The best possible evaluation of the non-thermal neutron flux is obtained if our data are combined with information on the shape (the spectrum normalization is left free) of neutron spectra measured at machines in the PSI energy range. An example of such a spectrum is presented in table 3 [14]; we are now trying to collect some more information on neutron measurements at intermediate energy machines. If

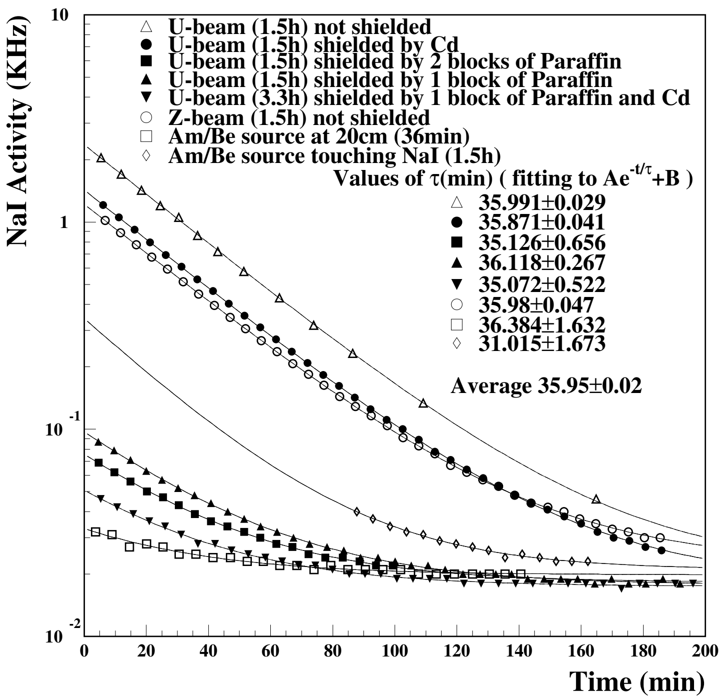

Figure 13: NaI decay curves.

use is made of such information and under the hypothesis of a roughly directional flux of energetic neutrons coming from the machine, one obtains for the flux of non-thermal neutrons:

$$\Phi_{nth} = 400 \quad \Phi_{nth}^{max} = 800 \quad \Phi_{nth}^{min} = 200 \quad n\ cm^{-2} s^{-1} \ .$$

Additional information on the neutron spectrum is contained in the data we took with the NE110 scintillator blocks; those data are still under analysis since a rather complex Monte Carlo simulation is essential for their interpretation. A different approach we tried to use to gain new information on neutrons is based on the neutron activation of targets having “threshold reactions”, namely reactions which have a sudden rise of the cross section at a fixed and known energy; the induced activity is then measured by detecting characteristic γ-lines with a Ge-detector.

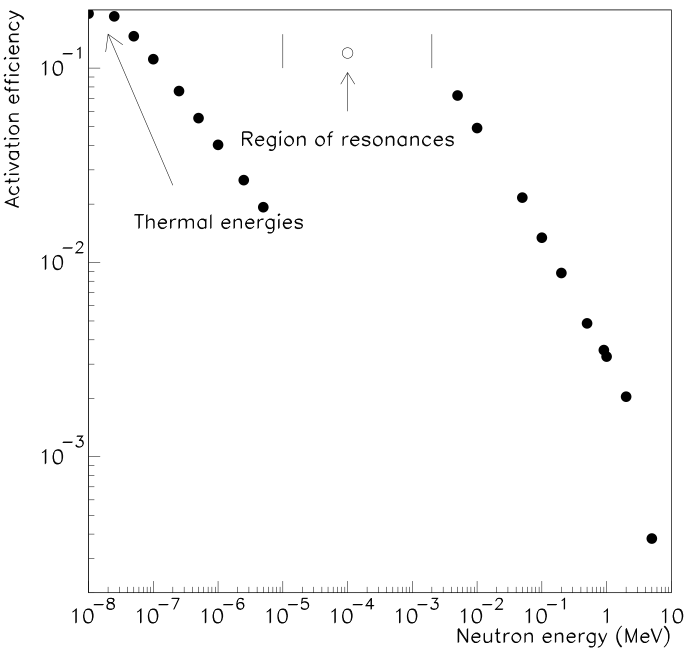

Figure 14: Neutron activation efficiency in NaI as a function of energy

A first attempt had too low a sensitivity; we shall try again and shall activate new targets chosen from the ones presented in table 4.

4.2 Gamma background

We measured the experimental area γ-background at several locations with a small $4'' \times 4''$ and a large $11'' \times 13''$ NaI crystal. An energy spectrum (small NaI crystal; energy resolution 3.4 % FWHM at the 2.5 MeV ^{60}Co sum-line) with no beam in the area is shown in fig.15; the typical γ-lines of the natural radioactivity background can be clearly recognized (^{238}U, ^{232}Th families and ^{40}K); the integrated rates are the ones of a "normal" laboratory; this background varies with the direction (lead shielded NaI with an entrance lead collimator) by up to a factor

Table 3: Example of an experimental neutron spectrum; 660 MeV proton beam.

Energy range (MeV)	**Fraction** (%)
$10^{-8} \div 4 \times 10^{-7}$	21
$4 \times 10^{-7} \div 10^{-1}$	10.5
$10^{-1} \div 2$	10
$2 \div 20$	19
> 20	39.5

Table 4: Properties of neutron activation targets.

Element	**Reaction**	**half-life**	**Threshold (MeV)**	**γ-Energy (keV)**	**γ-branching** (%)
^{115}In	$(n,n^{'})$	4.48 h	0.5	336.2	45.9
^{57}Ni	$(n,2n)$	36.08 h	12.6	1337.6	77.9
^{92}Nb	$(n,2n)$	10.25 d	8.8	934.5	99.9
^{52}Mn	$(n,4n)$	5.6 d	31.8	700	90
				1430	100

of three; it is larger when looking towards the machine, probably more because of the amount of concrete shielding than because of the area material activation. The measurement of the beam-on background, obtained with the large NaI crystal (collimator 10×10 cm^2) is shown in fig. 16; the large NaI is preferable because it fully contains the e.m. energy, but the larger mass makes it more vulnerable to neutrons. Fig. 16 A) is with the NaI collimator open, fig.16 B) is with the collimator closed by 10 cm thick lead bricks; fig. 16 C) is the integral spectrum of fig. 16 A). One can see that neutrons are giving a large contribution corresponding to thermal n-capture by ^{127}I (see the region $6 \leftrightarrow 7$ MeV; the spectra have also some contributions from pile-up effects. It is difficult to separate γ's from neutrons; one can therefore say that an abundant and degraded γ radiation is present in the region $1 \leftrightarrow 3$ MeV; at higher energies one can read the integral C) spectrum as giving an upper limit for the γ background, as a function of energy.

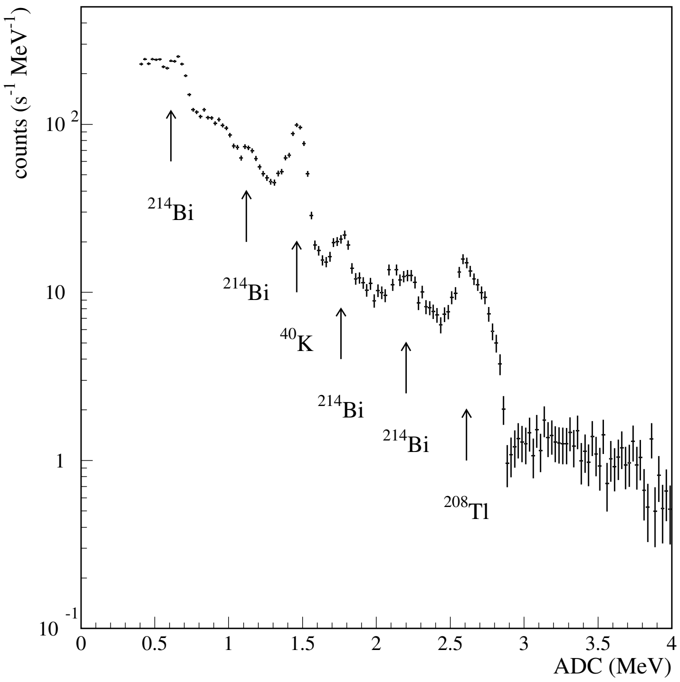

Figure 15: Radioactivity background measurements with the small NaI detector.

5 Preliminary results of a LYSO pre-shower prototype for the photon calorimeter

Two LYSO (70/30) crystals with dimensions $10 \times 5 \times 2\ cm^3$ were ordered from Crystal Photonics Inc. (Sanford, Florida), to be used in a pre-shower prototype. Unfortunately, one of the crystals broke during cutting and will be replaced by two $5 \times 5 \times 2\ cm^3$ crystals by the middle of June. By that date the mechanics with 36 readout channels will become available as well. We studied the available crystal with a single $2''$ photomultiplier, coupled to one $5 \times 2\ cm^2$ side through a plexiglass light guide. Various tests with radioactive sources, and 50 MeV protons, positrons and photons have been made, using the large NaI(Tl) crystal mentioned

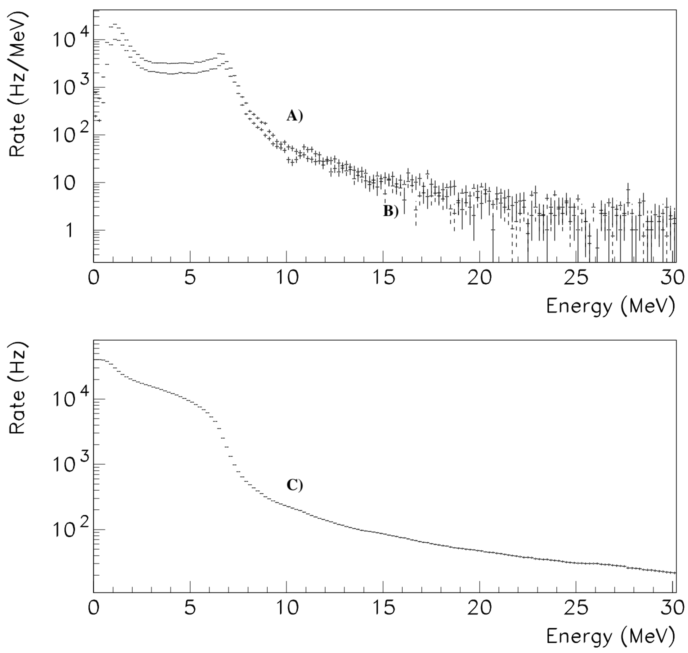

Figure 16: Measurements of the beam-on background.

above as stop detector. This detector was in fact designed to be used with a preshower detector and has a 0.2 mm aluminum window in front. The results will be described in the following subsections.

5.1 Non-uniformities and response to 50 MeV protons

The uniformity of the light yield was tested with a narrow proton beam (5 mm diameter) tuned to 50 MeV. The results are shown in table 5. Variations of order $\pm5\%$ are seen, which is in the range predicted by the manufacturer. For the proposed position-sensitive readout scheme this dependence could easily be corrected and it is expected that the new crystals, which resulted from a cut perpendicular to the direction of crystal growth, should be more uniform.

Table 5: Result of light yield scan of the LYSO crystal. Shown is the peak position of 50 MeV protons in a 10 mm grid (normalized to 100).

90	88	89	91	89
89	89	90	91	90
89	90	90	91	90
90	92	92	91	91
92	92	91	92	92
93	92	90	92	94
94	91	89	92	95
96	92	90	93	97
98	92	91	94	99
98	94	92	96	100

Fig.17 shows the response function for a well-focused proton beam. The otained energy resolution is 2.5 % FWHM with an unknown contribution from the beam.

5.2 Response to 50 MeV positrons

First the response of the NaI(Tl) detector alone was checked. Positrons were selected by a small trigger counter mounted at the center of the detector. The result, presented in Fig.18. shows a resolution of 6.0 % FWHM, which is very similar to the value measured in 1977 when the crystal was produced. Modern crystals show much better resolution [15] and we intend to order one such crystal as integral part of a more realistic prototype.

Next the LYSO crystal was mounted at 3.5 cm from the NaI(Tl) detector and the signals were added electronically after gain adjustment. The response of the combination of detectors is shown in Fig.19. The resolution (8.5 % FWHM) is worse than expected from the performance of the individual detectors. The Monte Carlo simulation, briefly described in the following section, explains this result which is caused by the finite distance between the LYSO and the NaI.

5.3 Response to 55 MeV photons

We tested the response of an almost full size element of the calorimeter to photons with energies close to 52.8 MeV.

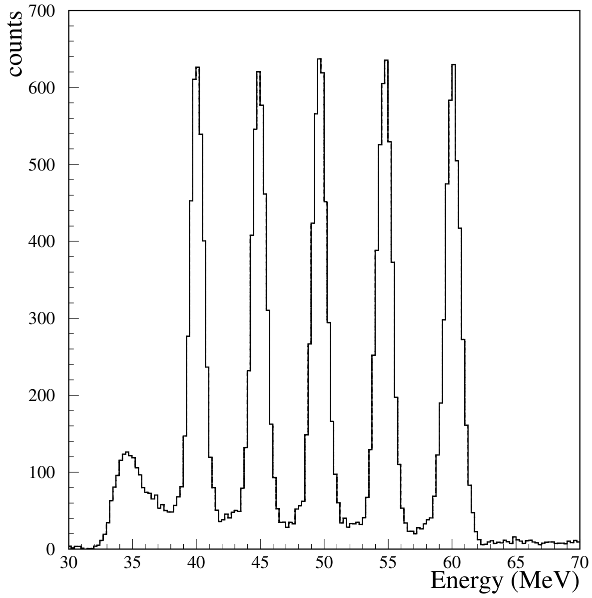

Figure 17: LYSO response function for protons of different energies. The energy resolution amounts to 2.5 % FWHM at 50 MeV.

For this purpose we used 150 MeV/c π^-'s which were brought to rest in a polyethylene target where π^0's were produced in the reaction

$$\pi^- + \mathrm{p} \rightarrow \pi^0 + \mathrm{n} \tag{4}$$

π^0's from this reaction are emitted isotropically with a 28 MeV/c momentum. Photons from π^0 decay have a 180° relative angle only if they are emitted along the π^0 line of flight; since the pion momentum is fixed, the energies of these photons are fixed: 55 and 83 MeV. By using two calorimeters at an angle of 180° relative to each other, one can select the 83 MeV photon in one calorimeter and look at the energy response to the 55 MeV photon in the other calorimeter.

For this measurement we used a LYSO crystal ($5 \times 10 \times 2$ cm^3) read laterally by a single 2" PMT and two calorimeters of cylindrical shape: a NaI(Tl) (28 cm diameter and 33 cm length) and a CsI(Tl) (15 cm diameter and 20 cm length).

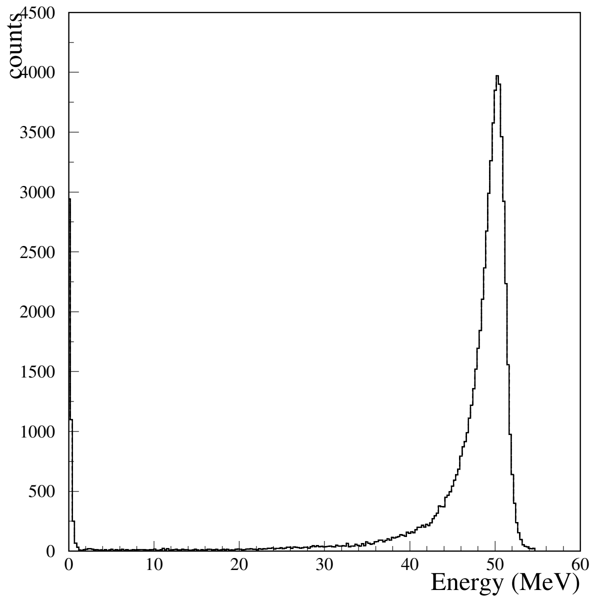

Figure 18: NaI(Tl) response function for 50 MeV positrons. The energy resolution amounts to 6.0 % FWHM.

The NaI is read by seven 2" PMT's while the CsI by one 13 cm diameter PMT. The lengths of the NaI and CsI calorimeters correspond to about 12 radiation lengths. The lateral shower containment is better for NaI since its radius corresponds to 3 Moliere radii (RM) while the CsI radius is about 2 RM.

We used an acquisition system based on a VME CPU board (based on a Motorola 68030 processor) which could read the total charge and time of our three experimental devices by means of VME ADC's and TDC's. The start to the TDC's was given by the coincidence of two plastic scintillators put on the π^- beam.

In a first measurement we utilized only the NaI and CsI calorimeters, both pointing at the target from a distance of $\sim 1\ m$ and with a relative angle of $180°$. Lead collimators ($10 \times 10\ cm^2$ for NaI and $5 \times 5\ cm^2$ for CsI) were put in front of both calorimeters.

These set–up conditions were particularly good since only photons interacting in a small region around the center of the calorimeters were selected.

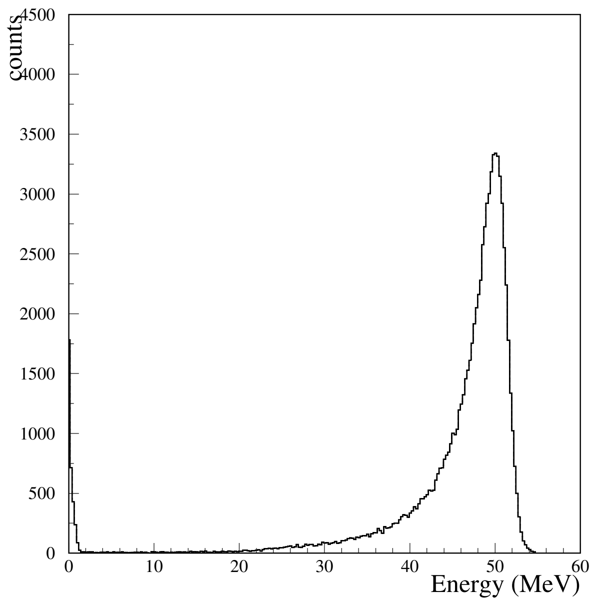

Figure 19: Response function of the NaI(Tl)+LYSO hybrid system for 50 MeV positrons. The energy resolution amounts to 8.5 % FWHM.

The readout trigger was a time-coincidence between the two calorimeters and a beam counter.

Time-of-flight measurement (especially in the NaI case, in which we used a constant fraction discriminator) gives a good separation of photons from background neutrons.

In fig.20 A) we show the energy deposited in the NaI vs. that deposited in CsI, after eliminating the neutron background, for a run of about 9.5 hours. The two photon peaks are clearly visible. By selecting the high energy peak in CsI we get the energy distribution measured in the NaI calorimeter for the 55 MeV photon; this is presented in fig.20 B). By fitting this distribution with an asymmetric curve (the fit is shown in the picture) we estimate a FWHM of (7.8 ± 1.2) %. The dimensions of the NaI crystal and the geometry in which it was used are such that a small fraction of the shower is not contained; we studied this effect with a GEANT based Monte Carlo simulation (which did not yet include light collection); the response

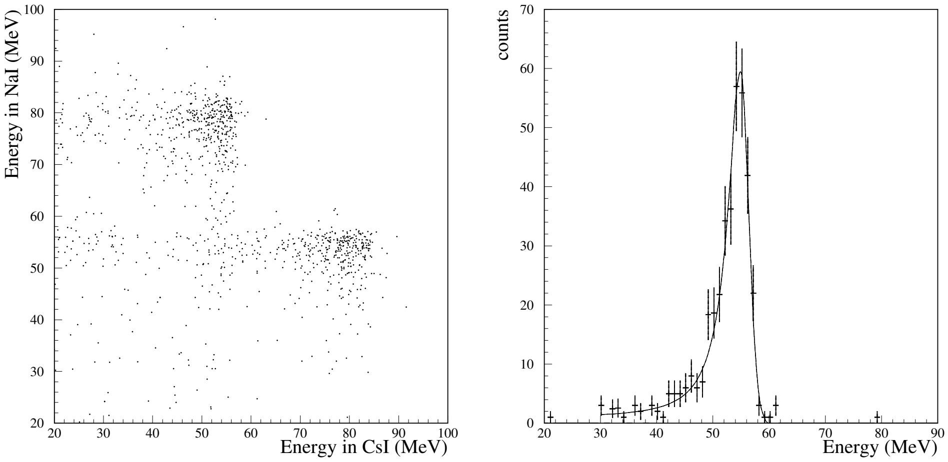

Figure 20: Calorimeters at about 1 m from the target: (left: A) NaI energy versus CsI energy; (right: B) Energy response of NaI to 55 MeV photons.

to a given energy loss in the calorimeter was smeared with a gaussian resolution function ($\sigma_E/E = 12\,\%/\sqrt{E(MeV)}$), needed to reproduce the NaI response for 50 MeV positrons (at the detector center), presented in section 5.2. The Monte Carlo simulation predicts an energy resolution of 6.3 % FWHM for 55 MeV γ's (5 % FWHM, if only the right part of the distribution is fitted with a gaussian). The difference between measurements and predictions might be partially due to inhomogeneities of the NaI crystal (which is 22 years old) or to collimator effects; we intend to further investigate this point with the positron beam.

We changed the set–up, to increase the detector acceptance and the statistics; we used larger collimators and reduced the distance between the two calorimeters (the distance from the target and the collimator aperture, for the NaI and CsI crystals became 60 cm, 11×13 cm^2 and 75 cm, 7.5×7.5 cm^2 respectively). We obtained a larger statistics, but the effects of the NaI inhomogeneities might be larger. This new set–up was used to make a second measurement in which we put the LYSO crystal in front of the NaI at a distance of 3.5 cm.

The figures corresponding to 20 A) and B), in which we require no signal in the LYSO, are shown in figures 21 A) and B). The NaI energy distribution at 55 MeV is now much broader; its FWHM is $(10.3 \pm 0.4)\,\%$ (that reduces to $(7.3 \pm 0.3)\,\%$ if

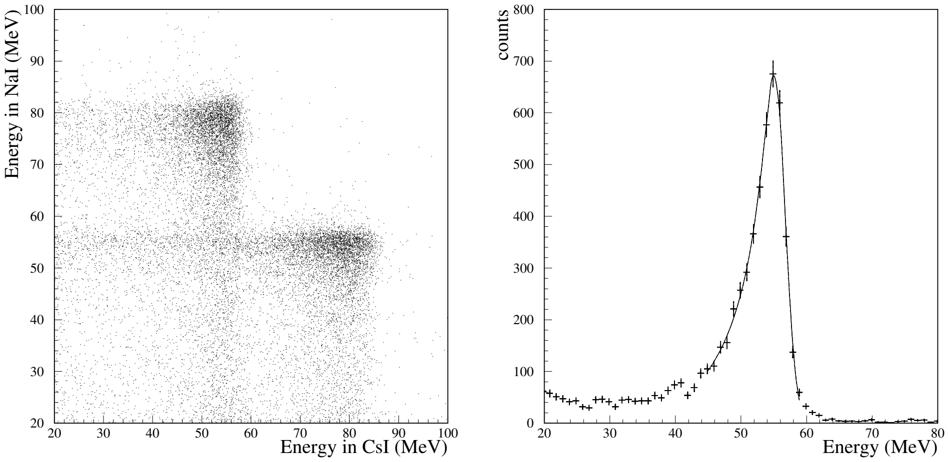

Figure 21: Calorimeters at a shorter distance from the target: (left: A) NaI energy versus CsI energy; (right: B) Energy response of NaI to 55 MeV photons.

we make a gaussian fit to the right part of the curve) which does not agree with the 6.6 % predicted by the Monte Carlo simulation.

If we now require a signal in the LYSO we get the energy distribution presented in fig.22; its FWHM is (9.3 ± 1.3) % (if we keep only the right part of the curve we end up with a FWHM of (6.7 ± 1.0) %). Within the statistics, this result is not much different from that of the NaI alone.

This first tests of the pre-shower detector was performed in combination with available detectors, one of them 22 years old. We plan to repeat these tests with the geometry foreseen for the experiment. For this purpose we will order a good and new NaI detector, with the LYSO crystal mounted in the "official" housing with 36 readout channels. Results should become available before the end of this year.

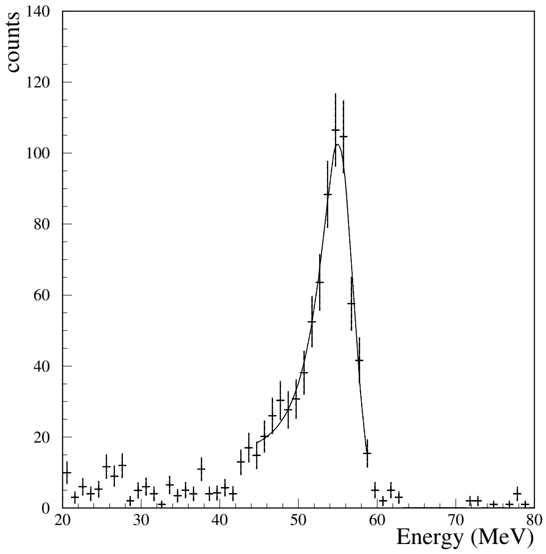

Figure 22: Energy response of NaI+LYSO to 55 MeV photons.

References

[1] MUEGAMMA Coll., Letter of Intent PSI R-98-05.0 (1998)

[2] S.M.Bar, Phys. Lett. B**448** (1998) 41.

[3] A.B.Arbuzov et al., Phys. Lett. B**432** (1998) 422.

[4] G.Couture et al., Eur. Phys. J. C**7** (1998) 135.

[5] MEGA Coll., hep-ex/9905013

[6] R.Lecomte et al., IEEE Trans.Nucl.Sci. B**45** (1998) 478

[7] O.Häusser et al., NIM B**213** (1983) 301

[8] L.C.Thompson, NIM B**25** (1964) 333

[9] L.Friedmann et al., Radio Chimica ACTA B**33** (1983) 183

[10] L.A.Schaller et al., Nucl.Phys. B**165** (1971) 415

[11] R.B.Firestone et al., Table of Isotopes, Wiley

[12] M.A.Lone et al., Atomic Data and Nuclear Data Tables B**26** (1981) 511

[13] V.Mc Lane et al., Neutron Cross Section, Academic Press

[14] V.E.Aleynikov et al., Inter.Cong on Protection Against Accelerator and Space Radiation. CERN (1971)

[15] A.Håkansson et al., NIM A**273** (1988) 211